ISBN: 978-3-95450-204-2 ISSN: 2673-5350 doi:10.18429/JACoW-IBIC2019-TUPP022

DEVELOPMENT OF THE CALCULATION METHOD OF INJECTION BEAM TRAJECTORY OF RIKEN AVF CYCLOTRON WITH 4D EMITTANCE MEASURED BY THE DEVELOPED PEPPER-POT EMITTANCE MONITOR

Y. Kotaka†, Y. Ohshiro, H. Yamaguchi, N. Imai, Y. Sakemi,
S. Shimoura, Center for Nuclear Study, University of Tokyo, Wako, Japan
T. Nagatomo, J. Ohnishi, T. Nakagawa, M. Kase, A. Goto, Riken Nishina Center, Wako, Japan
K. Hatanaka, Research Center for Nuclear Physics, Osaka University, Ibaraki, Japan
H. Muto, Suwa University of Science, Chino, Japan

Abstract

The Center for Nuclear Study, the University of Tokyo and RIKEN Nishina Center have been developing the AVF Cyclotron system at RIKEN. One of the important developments is to improve the transport system of the injection beam line. The transport efficiencies tend to decrease as beam intensities increase. To solve this problem, we developed the calculation method to trace a beam trajectory with a four-dimensional (4D) beam emittance measured by pepper-pot emittance monitor (PEM) as initial value. The reason for using the 4D beam emittance is that the transport system has rotating quadrupole magnets and solenoid coils, and that the space charge effect can be introduced. The beams through a pepper-pot mask can be detected on the potassium bromide fluorescent plate inclined 45 degree to the beam to be recorded by digital camera using developed PEM. We compared the calculated beam trajectory with the measurement of other beam diagnostics and quantified the degree of fit. It has been found that the degree of fit is improved by changing fiducial points on the fluorescent plate and optimizing the thickness of the fluorescent agent and the exposure time and gain of the digital camera.

INTRODUCTION

The Center for Nuclear Study, the University of Tokyo (CNS) and RIKEN Nishina Center have been expanding a variety of ion beams, increasing acceleration energy, and increasing beam intensity for RIKEN AVF Cyclotron [1, 2]. Among these, one of the important developments is to improve the transport system of the injection beam line.

Figure 1 shows injection beam line of AVF Cyclotron. Though there are 3 kinds of ion source, our target is 14 GHz electron cyclotron resonance ion source (ECRIS) named HyperECRIS developed by CNS.

According to the data from Sep. 2011 to Aug. 2013 when this study started, the average beam transport efficiency from 1st Faraday cup (FC_IH10) to 2nd Faraday cup (FC_I36), the center region, and the exit of extraction channel of accelerated beam were 64.7, 23.8, and 7.6 %, respectively. The center region is defined as the end of injection beam line. It is found most beams are lost in injection beam line, and these values tend to decrease as beam intensities of FC_IH10 increase.

However, all the transport efficiencies include the attenuation of 83 % by buncher mesh set over FC_I36. Moreover, as beam is compressed in the beam direction by the buncher and accelerated 6 times by the high frequency electrode to the end of center region, the beam dropping off the accelerating phase is lost. As the causes of beam loss in the injection beam line are complicated, it is necessary to improve this beam trajectory.

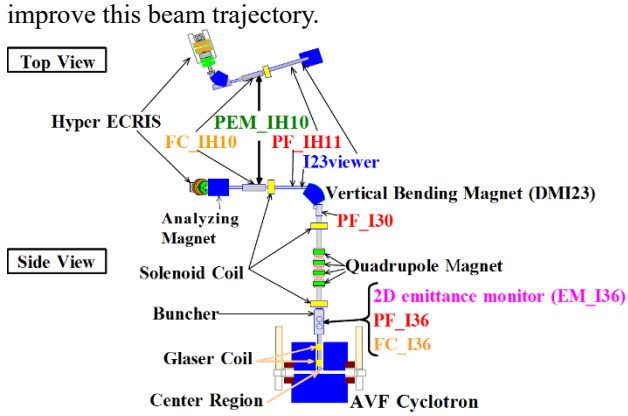

Figure 1: The injection beam line of the RIKEN AVF Cyclotron.

As the first step, we tried to understand the real beam transverse motion and the causes of beam loss. For this purpose, beam trajectory calculation is necessary. However, existing beam trajectory calculation codes are not useful because the beam intensity distribution generated by ECRIS is not gaussian, which means statistical approach is impossible. Therefore, we tried to develop the beam trajectory calculation method using the measured beam intensity distribution in the transverse phase space (x, x', y, y') (4D emittance) as the initial value by Lunge-Kutta method. As the second step, we will design beam trajectories which constrain beam loss and match the beam acceptance of AVF Cyclotron. Now, we completed to develop the beam trajectory calculation method including space charge effect.

PEPPER-POT EMITTANCE MONITOR

One reason for 4D emittance is that there are solenoid coils in the injection beam line. Another is that the beam line from analysing magnet to vertical bending magnet

† kotaka@cns.s.u-tokyo.ac.jp

ISBN: 978-3-95450-204-2 ISSN: 2673-5350 doi:10.18429/JACoW-IBIC2019-TUPP022

(DMI23) is rotated 20 degree against quadrupole magnets in the vertical beam line shown in the top view of Fig. 1. Then, x and y components of beam are coupled.

To measure 4D emittance, we adopted pepper-pot emittance monitor (PEM) [3, 4]. Our PEM named PEM_IH10 is composed of pepper-pot mask and fluorescent plate shown in Fig. 2. The pepper-pot mask made of 0.5 mm thick copper plate has holes with a diameter of 0.3 mm which are arranged at 3 mm interval within a 50 mm diameter circle. The fluorescent plate is poured with potassium bromide (KBr) on the copper plate (80x80 mm^2) and tilted 45 degrees. Beams passing through the holes of pepper-pot mask stop and emit light on the fluorescent plate set 55 mm behind pepper-pot mask. The beam view is recorded by digital camera set perpendicular to beam direction. PEM_IH10 is set from lower right against beam direction and 150 mm behind FC_IH10 in the beam line.

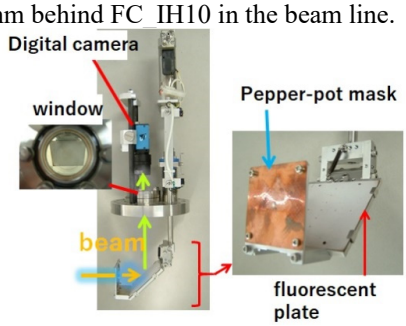

Figure 2: The schematic view of our PEM_IH10.

Optimizing Camera Lens Condition

We use Gigabit Ethernet (GigE) camera because of remote control. As the focal length of the chosen lens (TAMRON 13VM308AS) is 8 mm, we had to adjust object distance so as to keep the image resolution less than 0.1 mm/pixel and remove image distortion. The distortion can be measured with graph paper pasted on the fluorescent plate. We chose 225 fiducial points at 5 mm interval in 70x70 mm^2 on the graph paper, gave real positions in the beam line to fiducial points, measured the bitmap position of the fiducial points on the digital image, transformed the bitmap coordinates to the fiducial points coordinates using the projective transform coefficient, and defined the difference between fiducial points and their transformed position as distortion. When object distance was 250 mm, the distortion is shown in Fig. 3. The image resolution is 0.08 mm/pixel and the standard deviation of x and y is 0.08 and 0.07 mm, respectively. Angular accuracies are given by these standard deviations, and when the flight length is 55 mm, they become 2 mrad for both x' and y'. This performance was judged practical. This projective transform coefficient is also used in transforming beam images.

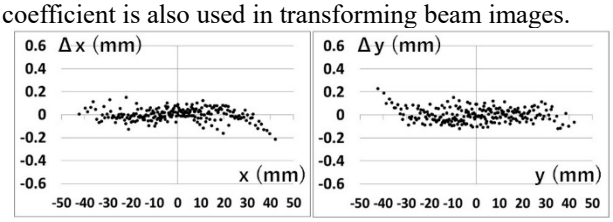

Figure 3: The distortion by optimized lens condition: x-axis (left) and y-axis (right).

THE DEVELOPMENT OF BEAM TRAJECTORY CALCULATION METHOD

Introducing Calculated 3D Magnet Field

The calculated 3D magnetic fields have been used for the beam trajectory calculation because they are essential in order to introduce space charge effect. As space charge effect depends on the beam intensity distribution on the (x, y) plane, it should be simultaneously integrated into the equation of motion (EOM) of the beam trajectory calculation together with real magnetic forth at any position of beam direction. That is to say, the fringe field of magnet cannot be neglected. The magnetic field of quadrupole magnets and DMI23 were calculated by TOSCA 3D [5] and solenoid coil were by FEMM [6].

Introducing Space Charge Effect

$$\frac{d^2x}{ds^2}=\frac{4\lambda r_p}{\beta^2\gamma^3 a(a+b)}(x-x_0)\quad \frac{d^2y}{ds^2}=\frac{4\lambda r_p}{\beta^2\gamma^3 b(a+b)}(y-y_0) \qquad (1)$$

$$\frac{(x-x_0)^2}{a^2}-\frac{2R}{ab}(x-x_0)(y-y_0)+\frac{(y-y_0)^2}{b^2}=1-R^2 \qquad (2)$$

Equation (1) is EOM of space charge effect. It is approved if the beam cross-section is ellipse, the transverse and longitudinal beam densities are uniform, and R is 0 in Eq. (2) which is the formula of ellipse [7]. In Eqs. (1) and (2), (x, y) is transverse phase-space coordinate, (x_0, y_0) is the center of ellipse, a and b are ellipse radii, s is beam axis, λ is the number of particles per unit length,β and γ are Lorentz factors, and r_p is the classical radius of ion.

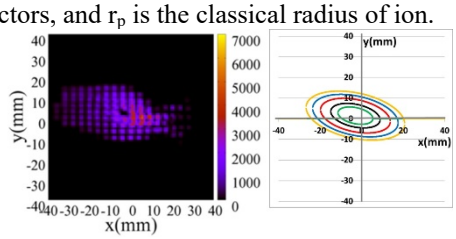

Figure 4: The left is a beam intensity distribution on (x, y) plane. The right is the ellipse given by Eqs. (2) with parameters calculated from the left distribution statistically. The differences of colors show multistep ellipses.

The left of Fig. 4 is a sample of a beam intensity distribution on (x, y) plane measured by PEM_IH10. Although its shape is not an ellipse, we approximate it to an ellipse. The values of (x_0, y_0) and R in Eq. (1) are given by calculating the average and correlation of the distribution. The values of (a, b) are given by multiplying the standard deviations of the distribution by an arbitrary number. When radii of a and b are equal to standard deviation of the distribution, we name the ellipse basic-ellipse. To approximate a beam intensity distribution by one ellipse is named single-ellipse model.

By the way, the ellipse is usually inclined, which means R is not 0. In order to use Eq. (1), R must be 0. In such a case, the (x, y) coordinate is rotationally transformed into a coordinate in which R is 0. In this coordinate, Eq. (1) can

ISBN: 978-3-95450-204-2 ISSN: 2673-5350 doi:10.18429/JACoW-IBIC2019-TUPP022

be made. At last, the Eq. (1) of this coordinate are inversely transformed to the original (x, y) coordinate.

Moreover, multistep-ellipse model was formulated to increase the accuracy. Multistep ellipses are made by changing its radii and keeping the center as shown in the right of Fig. 4. The way to make EOM is following. First, for the beam element in the innermost ellipse, Eq. (1) is constructed made from the innermost ellipse. Then, for the beam element stayed between the second and the first innermost ellipse, another Eq. (1) is made from the second ellipse. For the outer ellipses, the other Eq. (1) are constructed accordingly.

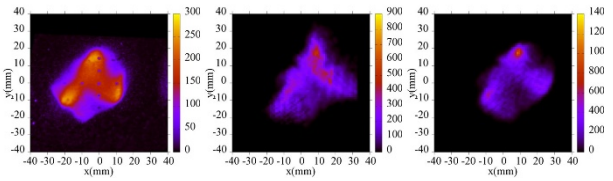

Figure 5: The left, middle, and right are the beam intensity distribution measured by I23viewer, calculated by the single-ellipse model, and calculated by the multistep-ellipse model, respectively.

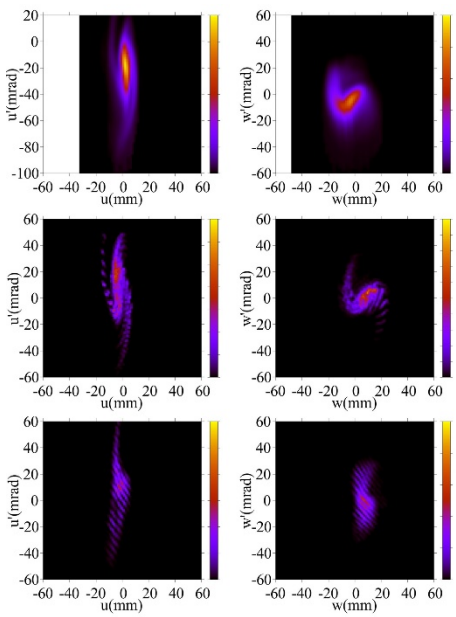

Figure 6: The left and right column show 2D emittances of the (u, u') and the (w, w'), resprctively. (Top) the measurement by EM_I36. (middle) The result of beam trajectory calculation to the position of EM_I36 by calculation including space charge effect. (bottom) The result of beam trajectory calculation to the position of EM_I36 excluding space charge effect.

The result of the single-ellipse and multistep-ellipse model is shown in Fig. 5. Test beam is 15.4 keV $^4He^{2+}$ of 124 eμA. The left, middle, and right of Fig. 5 are beam intensity distributions measured by beam viewer (I23viewer), calculated by the single-ellipse model, and calculated by the multistep-ellipse model, respectively. The radii of the single-ellipse model are 1.8 times larger than the radii of basic-ellipse. The multistep-ellipse model is composed of ellipses made by dividing 6 times the radii of basic-ellipse by 30 equally. It can be seen that the multistep-ellipse model reproduces the measured distribution better than the single-ellipse model.

Then, the necessity of considering the space charge effect is shown by comparing the measurement of 2D emittance monitor (EM_I36) with the beam trajectory calculation. The top row of Fig. 6 shows 2D emittance measured by EM_I36. The left and right columns show the beam intensity distribution in the (u, u') and (w, w') coordinate, respectively. The (u, w) coordinate of EM_I36 is perpendicular to beam direction and is rotated by 45 degree against (x, y) coordinate and the angles of u and w are indicated by u' and w', respectively. The coordinates of x and y are directed into the page and rightward in Fig. 1, respectively. The result including and excluding space charge effect are shown in the middle of Fig. 6 and the bottom of Fig. 6, respectively. The middle of Fig. 6 is similar to the top of Fig. 6, but the bottom of Fig. 6 is not. The space charge effect is necessary for the practical calculation.

EVALUATION METHOD

In order to evaluate the beam trajectory calculation numerically, we compare it with the measurement of other diagnostics by χ^2 test. We have I23viewer, beam profile monitor (BPM) and EM_I36 as diagnostics. As I23viewer and EM_I36 are 2D distribution, χ^2 should be calculated with 2D distribution. However, some 2D distributions made from the beam trajectory calculations become uneven because the position interval measured by PEM_IH10 is 3 mm. Consequently, the value of χ^2 becomes so large that a fair comparison is difficult. Therefore, the comparison by projections on the arbitrary coordinate made from 2D distribution was adopted. This way is preferable to prevent the distribution from being uneven.

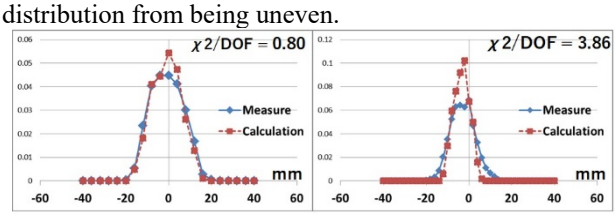

Figure 7: Examples of the degree of fit. The bule and red line shows the projection of the measurement and the beam trajectry calculation. The χ^2/DOFs (degree of fit) of left and right is 0.80 and 3.86, respectively.

Examples of the comparison by projections are shown in Fig. 7. The blue and red lines show the projection of the measurement and the beam trajectory calculation, respectively. The areas of both distributions are normalized to 1. By the way, the dispersion of χ^2 is the square of 10 % of the highest value of the measured distribution because our accuracy of beam trajectory calculation is rough. Our purpose is relative comparison among many kinds of beam trajectories. However, χ^2 divided by degree of freedom (χ^2/DOF) is adjusted to be about 1 when a beam trajectory calculation is judged to fit a measurement by visual judgement. Then, χ^2/DOF of the left and right of Fig. 7 is 0.8 and 3.86, respectively. This χ^2/DOF is named degree of fit.

ISBN: 978-3-95450-204-2 ISSN: 2673-5350 doi:10.18429/JACoW-IBIC2019-TUPP022

CAMERA CONDITION FOR THE THICNESS OF FLUORESCENT AGENT

A florescent palate is exchanged when deteriorated. Once, the degree of fit was larger when we changed to thicker florescent agent than before. We assumed that the amount of luminescence on the fluorescent plate increased relatively as the thickness was thicker and exposure time and gain of digital camera were not optimized. Then, we examined optimum exposure time (1/10, 1/20, and 1/38 seconds) and gains (5, 7, 9, 11, 13, and 15 dB) of digital camera with 2 kinds of thickness 1.9 and 34.6 μm by measuring the degree of fit given by 1st BPM (PF_IH11) using 23.6 keV $^4He^{2+}$ ion beam of 100 eμA. The thickness of florescent agent is defined by dividing the weight by the area and the density.

The results of the degree of fit are shown in Fig. 8. PF_IH11 measures beam profiles of y, u, and w direction. In this section, degree of fit is given by dividing the sum of χ^2 of y, u, and w by the sum of DOF of y, u, and w. Cells of less than 1.0 are filled with brown for 1.9 μm and with deep blue for 34.6 μm in Fig. 8. We found that even thicker thickness is useful when gain becomes lower and exposure time becomes shorter. In any case, it is necessary to optimize before measurement.

thicness 1.9 μm High ← Gain (dB) → Low

Exposure time (sec) long ↑ short ↓	15	13	11	9	7	5
1/10	1.33	0.97	0.77	0.68	0.63	0.68
1/20	0.91	0.8	0.69	0.65	0.79	1.1
1/38	0.81	0.63	0.64	0.81	1.43	1.73

thickness 34.6 μm High ← Gain (dB) → Low

Exposure time (sec) long ↑ short ↓	15	13	11	9	7	5
1/10	1.68	1.38	1.1	0.93	0.51	0.51
1/20	1.19	0.94	0.67	0.49	0.64	1.04
1/38	0.72	0.56	0.5	0.79	1.52	1.86

Figure 8: The degree of fit of PF_IH11 given when the thickness of fluorescence agent and the exposure time and gain of digital camera are varied. (top) thickness is 1.9 μm (bottom) thickness is 34.6μm.

BEAM TEST

In order to evaluate the developed beam trajectory calculation method, the degree of fit is examined by using 4 kinds of beam intensities (124, 187, 196, and 308 eμA) of 15.4 keV $^4He^{2+}$ and 2 kinds of beam intensities (100 and 214 eμA) of 12.6 keV $^2H^+$. The left and right of Fig. 9 indicate the scatter plot of the degree of fit of (u, u') and (w, w') of EM_I36, respectively. For both scatter plots, it is found that the degree of fit of positions are less than 4, but the 3 degree of fit of angles are more than 6. These three samples have the tendency that the widths of angular distributions of the beam trajectory calculations were smaller than ones of the measurements.

On the contrary, Fig. 10 shows the scatter plot of degree of fit of (u, w) of 3rd BPM (PF_I36) set 107.5 mm behind EM_I36. It is found that all the degree of fit are less than 4.2 and are not as large as ones imagined from Fig. 9. Probably, the measured angle of EM_I36 may be fault. They contain noise because the zero level of signal becomes uneven by secondary electrons made from beam.

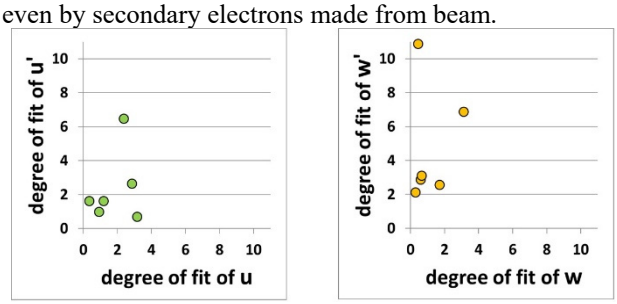

Figure 9: The left and right scatter plot shows the degree of fit of (u, u') and (w, w') compared with EM_I36, respectively.

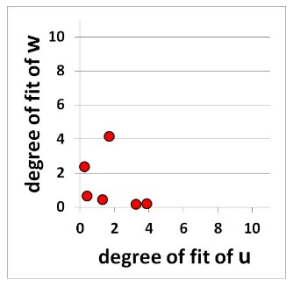

Figure 10: Scatter plot shows the degree of fit of (u, w) compared with PF_I36.

CONCLUSION

Because the degree of fit of PF_I36 and the position of EM_I36 reach less than 4.2, the developments of PEM_IH10 and beam trajectory calculation method can be judged to be used in practical way. Accordingly, we can start the 2nd step which is to design the beam trajectory suitable for the acceptance of the AVF cyclotron and to constrain beam loss. At the same time, we will examine the degree of fit of various ion species, beam intensity, and energy to see measurement limit. Moreover, longitudinal motion of beam will be considered as necessary.

REFERENCES

[1] Y. Kotaka *et al.*, "Development of Low-Energy Heavy-Ion Beams by the RIKEN AVF Cyclotron and Hyper ECR Ion Source of CNS", in *Proc. 13th Int. Conf. on Heavy Ion Accelerator Technology (HIAT'15)*, Yokohama, Japan, Sep. 2015, paper MOPA10, pp. 58-61.

[2] J. Ohnishi, A. Goto, M. Kase, and Y. Kotaka, "Study on Energy Upgrade and Beam Transmission Efficiencies for RIKEN K-70 AVF Cyclotron", in *Proc. 21th Int. Conf. on Cyclotrons and their Applications (Cyclotrons'16)*, Zurich, Switzerland, Sep. 2016, pp. 332-335. doi:10.18429/JACoW-Cyclotrons2016-THP13

[3] T. Hoffmann, D. Ondreka, A. Peters, A. Reiter, and M. Schwickert, "Beam Quality Measurements at the Synchrotron and HEBT of the Heidelberg Ion Therapy Center", in *Proc. BIW'08*, Lake Tahoe, CA, USA, May 2008, paper TUPTPF044, pp. 210-212.

[4] L. E. Collins and P. T. Stroud, *Nucl. Instr. and Meth.* 26 (1964), p. 157-166.

[5] https://operafea.com

[6] D. C. Meeker, http://www.femm.info

[7] S. Y. Lee, Accelerator Physics 1st ed. (World Scientific, Singapore, 1999).